Faraday Discussions
Cite this: *Faraday Discuss.*, 2026, **263**, 294

PAPER

The use of kraft lignin to enhance nanocellulose film properties†

Raquel Martín-Sampedro, *[a] Antonio Ovejero-Pérez, ‡[b] Mercedes Oliet, [b] Virginia Alonso, [b] Francisco Rodríguez, [b] David Ibarra [a] and María E. Eugenio *[a]

Received 30th April 2025, Accepted 27th June 2025
DOI: 10.1039/d5fd00063g

The pressing need to replace petroleum-based plastics with renewable and biodegradable alternatives has sparked growing interest in biopolymers derived from lignocellulosic biomass as sustainable solutions. Among these, nanocellulose stands out as a versatile product capable of forming strong, transparent, and flexible films. However, these films lack active properties like antioxidant, antibacterial and UV-shielding capacity, essential for applications such as food packaging. To address this, incorporating lignin, a byproduct of lignocellulosic biorefineries, offers a promising route to enhance the functionality of nanocellulose films. In line with this idea, this work studies the incorporation of kraft lignin into nanocellulose films by two different protocols: the first protocol involves directly mixing a cellulose nanofiber (CNF) suspension with an aqueous lignin suspension; the second protocol uses lignin dissolved in acetone : water (9 : 1) which is transformed into lignin nanoparticles (LNPs) *via* solvent shifting when mixed with the aqueous CNF suspension. The resulting suspensions of CNFs and lignin were subsequently used to produce casting films. It was found that incorporating lignin into the CNF film not only conferred UV-shielding capacity, but also enhanced barrier properties without compromising the mechanical properties, particularly when lignin was introduced as LNPs (even at 10–20% LNP content). However, adding bulk lignin at a high concentration (20%) negatively affected water vapor permeability and mechanical properties. Antioxidant and antibacterial capacities correlated with lignin content, showing greater enhancement when lignin was present as nanoparticles compared to bulk lignin. These results indicate that forming LNPs *in situ* within the CNF suspension is a more effective approach to optimize the properties of nanocellulose films. Thus, the

[a]*Institute of Forest Science (INIA-CSIC), Ctra. de la Coruña Km 7.5, 28040 Madrid, Spain. E-mail: raquel.martin@inia.csic.es; mariaeugenia@inia.csic.es*
[b]*Complutense University of Madrid, Av. Complutense s/n, 28040 Madrid, Spain*

† Electronic supplementary information (ESI) available: Fig. S.1. FTIR spectrum of nanocellulose–lignin films. Table S.1. Characteristic parameters from thermogravimetric analysis of the nanocellulose–lignin films. See DOI: **https://doi.org/10.1039/d5fd00063g**

‡ Present address: Department of Chemical Engineering, Imperial College London, South Kensington Campus, Exhibition Road, London SW7 2AZ, UK.

obtained films presented good active properties with mechanical properties comparable to those of traditional plastics, but significantly lower barrier properties.

1. Introduction

Nowadays, the extensive use of non-biodegradable plastics is seriously threatening the environment and also human health.[1,2] On the one hand, the production of these plastics is based on fossil resources, which not only implies environmental problems related to non-renewable raw materials and polluting production processes (with associated emission of greenhouse gases), but also a high dependence on the price of petroleum oil and natural gas. On the other hand, the use of plastic is linked to serious environmental problems regarding the disposal of non-biodegradable waste and the accumulation of microplastics, with associated health problems. Therefore, the search for more environmentally friendly materials based on renewable resources is crucial for today's society.[1] These new materials, called bio-plastics, should also be biodegradable, non-toxic, and low-cost. Some of the proposed bio-plastics are polysaccharides (such as chitosan, starch or cellulose), proteins (such as keratin, collagen, gelatin or soy protein), polyesters (such as polyhydroxybutyrate (PHB)), or polylactides (such as polylactic acid (PLA)).[2]

Among polysaccharides, nanocellulose stands out due to its high strength and optical transparency, low density and lack of toxicity.[3,4] Furthermore, it offers an extensive surface area with highly versatile surface chemistry.[3,5] Nevertheless, the lack of active properties, such as antioxidant or antimicrobial capacities, limits its application in some sectors such as food packaging or medical applications. To overcome this limitation, active components can be incorporated into the nanocellulose matrix. In the case of food packaging, natural compounds such as essential oils, phenolic compounds, chitosan or nisin have been added into different bio-plastic matrices in order to obtain packaging materials able to protect the food from oxidation and microbial degradation.[2] Lignin has also been studied as an active compound, achieving materials not only with antioxidant and antimicrobial capacities but also UV-shielding ability.[1,6]

Lignin is one of the most abundant natural polymers found in lignocellulosic materials such those from trees as well as agricultural and forestry residues. The main source of lignin is the pulp and paper industry, especially kraft pulping mills, which produce annually around 50–60 million tons of kraft lignin.[2] In this industry, kraft lignin is a residue in the production of cellulose kraft pulp. Black liquor, containing this residual lignin, is incinerated to produce heat and electricity, using approximately 40% for self-supply and the remaining 60% for sale.[7] In order to increase the profitability and sustainability of the pulp and paper industry, several alternative uses of lignin in novel materials or chemicals have been investigated in the past decades. For this purpose, it is crucial to understand the complex chemical structure of lignin, which impacts lignin properties and is dependent on the lignin source and isolation procedure,[8,9] and thus will define its potential uses.[10] Its polyaromatic structure with several different functional groups endows lignin with active properties, *i.e.*, antibacterial and antioxidant properties are attributed to phenolic groups as well as functional groups with oxygen such as methoxyl groups.[6,11,12] Likewise, the UV-shielding ability is linked to phenolic and conjugated

carbonyl groups.[6,13,14] Furthermore, lignin properties also depend on the morphology of lignin. In fact, several authors have reported higher active properties (including UV-shielding, antioxidant and antibacterial capacities) of composites with lignin nanoparticles (LNPs) compared to those with bulk lignin.[15–17] Most of these authors followed a two-step procedure to introduce the LNPs into the polymeric matrix. In the first step, LNPs are normally formed by solvent shifting, pH shifting or crosslinking/polymerization, although other methods, such as mechanical treatment, ice-segregation, aerosol processing, *etc.*, have also been reported.[7] Once the lignin nanoparticles are formed, they can be chemically modified or directly added to the polymeric matrix in a second step. Only a few authors have studied the formation of lignin nanoparticles directly on the polymeric matrix, merging the formation and addition steps in a single step.[18]

The objective of the present work is to study the effect of the addition of lignin into cellulose nanofiber films, regarding its influence on mechanical, thermal, optical, barrier and active properties (antioxidant, antibacterial and UV-shielding capacities). Apart from varying the dose of lignin added into the nanocellulose–lignin film, two different protocols of lignin addition prior of the formation of films have been studied to evaluate the influence of the lignin morphology. The first protocol allowed the addition of bulk lignin suspension, while the second one allowed the formation of lignin nanoparticles *in situ* within the nanocellulose suspension (by solvent shifting). This second protocol simplifies the most commonly used procedure, in which lignin nanoparticles are first formed in an aqueous suspension and afterwards added to the nanocellulose suspension, making its industrial application easier.

2. Materials and methods

2.1. Materials

Bleached kraft pulp and black liquor were kindly supplied by La Montañanesa pulp mill (Lecta Group, Spain). The raw material used by this pulp mill was *Eucalyptus globulus*.

All chemicals were purchased from Sigma-Aldrich (Madrid, Spain) or Fisher Scientific (Madrid, Spain).

2.2. Cellulose nanofiber production

Cellulose nanofibers (CNFs) were produced from never-dried bleached pulp after a carboxylation pretreatment *via* TEMPO-mediated oxidation followed by microfluidization. Carboxylation was performed at room temperature and 1% (w/v) pulp consistency, using 0.013 g of NaClO, 0.016 g of TEMPO (2,2,6,6-tetramethylpiperidine-1-oxyl radical) and 0.1 g of NaBr per gram of dry pulp. 0.5 M NaOH was used to maintain the pH at 10. Reaction was finished when no drop in pH was observed. Then, oxidized fibers were washed by filtration with deionized water until at neutral pH and subjected to 4 passes in a microfluidizer M-110 EH (Microfluidics Corp., USA). In the first pass, an interaction chamber of 200 μm was used, while in the rest of the passes two sequential chambers of 200 μm and 100 μm were used. The resulting CNFs presented a carboxyl content of 1043 ± 150 μmol g^{-1} and a mean nanofiber diameter of 5.0 ± 1.4 nm.

2.3. Kraft lignin extraction

Kraft lignin was extracted from the black liquor *via* acid precipitation, adding concentrated sulfuric acid drops under stirring until pH 2.5 was reached. Precipitated kraft lignin was separated from the liquid fraction by centrifugation at 12 000 rpm for 10 min. Then, it was washed with acidified water (pH 2.5) and separated by centrifugation 4 times. Finally, it was dried at 40 °C under vacuum and homogenized in an agate mortar.

2.4. Nanocellulose–lignin film formation

Two different protocols were followed for the preparation of the nanocellulose–lignin films, differing in the method used to prepare the lignin suspensions/solutions. In the first one, 0.3% (w/v) kraft lignin aqueous dispersion (at pH 8) was prepared using a Miccra D-1 high-shear homogenizer (Miccra GmbH, Germany) equipped with a Miccra Pico DS-14-P disperser (3 min at 20 000 rpm). In the second one, kraft lignin was dissolved in 9 : 1 acetone : water to a final concentration of 0.3% (w/v) by magnetic stirring. Then, the lignin suspension/solution was slowly added to 0.3% aqueous CNF suspensions under magnetic stirring. Lignin–nanocellulose volume ratios were adjusted in order to prepare mixtures with 0%, 2.5%, 5%, 10% and 20% lignin content (w/w with respect to the total mass of dry film). The mixtures were magnetically stirred for 60 min before preparing the films *via* casting (65.1 mL of each mixture was placed in a 90 mm Petri dish and dried at 30 °C for several days until at constant weight). The films formed from the aqueous dispersion of lignin were labeled as CNF-*X*L, where *X* indicates the percentage of lignin. When lignin was dissolved in acetone : water (second protocol), its addition into an aqueous CNF suspension promoted the formation of lignin nanoparticles (LNPs) by solvent shifting. Thus, films prepared *via* this protocol were labeled as CNF-*X*LNP, where *X* also indicated the percentage of lignin.

2.5. Characterization of nanocellulose–lignin films

The surface morphology of the films was studied *via* scanning electron microscopy (SEM) using a JEOL JSM 6335 F microscope at an operation voltage of 5.0 kV. Gold sputtering onto the sample surface was used to impart electrical conductivity. Analyses were developed in the technical facilities of the Spanish National Centre for Electron Microscopy (Madrid).

FTIR spectra of the films were directly acquired using a JASCO FT/IR 460 Plus spectrometer (JASCO, Japan). Spectra were obtained in the 4000–600 cm^{-1} spectral range with a resolution of 1 cm^{-1} and 400 scans.

Thermogravimetric analysis (TGA) was performed under a nitrogen atmosphere in a TG Mettler Toledo instrument TGA/SDTA851e using alumina crucibles. A first drying step was carried out from room temperature to 105 °C, maintaining this last temperature for 30 min. Then, the temperature was increased to 800 °C at a heating rate of 10 °C min^{-1}.

2.6. Water solubility and swelling capacity of nanocellulose–lignin films

Solubilization of the films in water was evaluated by placing a piece of each film (of known dry weight) in distilled water and keeping them under stirring for 24

hours at 22 °C. Then, the films were removed and dried in an oven at 105 °C. Solubility was determined by comparing the dry weight of the film before and after water immersion.

The swelling capacity of the films was determined by submerging a piece of each film in distilled water for 24 hours without stirring. The swelling capacity was calculated as the total water retention per gram of dry film, determined by weighing the wet film after removing the excess water with filter paper, and the dry film after drying in an oven at 105 °C.

2.7. Water vapor permeability of nanocellulose–lignin films

The water vapor permeability (WVP) of the films was determined to evaluate their gas barrier properties. The desiccant method was followed according to the ASTM E96 standard. Films were mounted in test cells covering the 1 cm diameter hole of their lids. Anhydrous calcium chloride was used inside the test cell to maintain a 0% relative humidity, while the relative humidity outside was fixed at 75% by placing the test cells into a humidity chamber. Tests were performed at room temperature over 4 days, following the weight gains every 24 hours. At least three repetitions for each film were carried out. The weight gain of each film was plotted *versus* time, and the water vapor transmission rate (WVTR) was calculated by dividing the slopes of these curves by the exposed film area. WVP was determined according to eqn (1), taking into account the thickness of each film (L, mm) and the partial water vapor pressure difference on both sides of the film (ΔP, kPa):

$$\mathrm{WVP} = \frac{(\mathrm{WVTR} \times L)}{\Delta P} \tag{1}$$

2.8. Mechanical properties of nanocellulose–lignin films

The mechanical properties of the films were determined *via* tensile tests performed using an MTC-100L Universal Testing Machine (IDM, Spain). Young's modulus, tensile strength and elongation at break were calculated from the strength *vs.* elongation curves for each type of film. Test pieces of 40 × 10 mm were tested using an initial grip separation of 25 mm and a crosshead speed of 1 mm min^{-1}.

2.9. Optical properties of nanocellulose–lignin films

Total transmittance and diffuse transmittance between 200 and 800 nm wavelengths were determined for each film using a Lambda 365 UV-vis spectrometer (PerkinElmer, USA) with an integrating sphere. From these data, opacity (at 600 nm), transmission haze (at 600 nm) and UV-shielding capacity (between 400 and 200 nm) were estimated.

Color coordinates (CIE $L^*a^*b^*$) were also determined using an ELREPHO 070 spectrophotometer (Lorentzen and Wettre, Sweden). Due to the transparency of most of the films, white paper ($L^* = 97.9$, $a^* = -0.2$ and $b^* = 2.4$) was placed under the film when measuring. The color change due to the addition of lignin was evaluated according to eqn (2), where the "CNF" subscript indicates the color coordinates for the CNF film without lignin, and the "i" subscript indicates the color coordinate of each film sample.

$$\Delta E_i = \sqrt{(L_{CNF} - L_i)^2 + (a_{CNF} - a_i)^2 + (b_{CNF} - b_i)^2} \quad (2)$$

2.10. Antioxidant capacity of nanocellulose–lignin films

The radical-scavenging ability of each film was evaluated following the $ABTS^{+\bullet}$ method[19] in order to determine the antioxidant capacity of the films. A 7 mM ABTS (2,2′-azinobis(3-ethylbenzothiazoline-6-sulfonic acid)) aqueous solution was prepared, and potassium persulphate at a final concentration of 2.45 mM was added. The reaction mixture was placed in the dark at room temperature for 16–24 hours to allow the formation of $ABTS^{+\bullet}$ radicals. Then, the mixture was diluted with 5 mM phosphate buffer (pH 7.4) until an absorbance of 0.70 ± 0.02 at 734 nm was reached. 2.5 mL of the resulting solution was placed in a cuvette and a piece of the film (between 1 and 0.3 mg) was submerged in the solution and thoroughly mixed in a vortex. The absorbance of the mixture at 734 nm was registered over 6 min using a Lambda 365 UV-vis spectrometer (PerkinElmer, USA), determining the percentages of inhibition (% I) for each film as the difference between the absorbance of the solution prior to the addition of the film (A_i) and 6 min after the addition ($A_{6\ min}$) (eqn (3))

$$\%\ I = \frac{(A_i - A_{6\ min})}{A_i} \times 100 \quad (3)$$

The antioxidant capacity of each film was determined by comparing the percentages of inhibition caused by the film with those caused by standard solutions of Trolox (6-hydroxy-2,5,7,8-tetramethylchroman-2-carboxylic acid). Thus, the antioxidant capacity was expressed as mg of Trolox equivalent (TE) per g film.

2.11. Antibacterial activity of nanocellulose–lignin films

A Gram-positive bacterium (*Staphylococcus aureus*, CECT 231) and a Gram-negative bacterium (*Escherichia coli*, CECT 433) were used to evaluate the antibacterial activity of the nanocellulose–lignin films. Nutrient broth (NB) and Lennox Luria Bertani broth (LB) were used as the culture media for *S. aureus* and *E. coli*, respectively. Inoculums were prepared by growing one bacterial colony forming unit (CFU) in the corresponding liquid culture medium at 37 °C and 140 rpm for 16 h. 40 μL of these inoculums were added to sterile tubes containing 2 mL of LB or NB medium and a piece of each film (30 mg). Controls without film were also assayed. At least three replicates for each film were prepared. After 24 h of incubation at 37 °C and 140 rpm, serial dilutions (in phosphate buffer) of the resulting cultures were prepared and spread on agar medium plates. These plates were incubated for 24 h at 37 °C and the number of bacterial CFUs was counted. The antibacterial activity of each film was evaluated according to the log reduction ($\log R$), which is related to the relative number of living bacterial that are eliminated by the film's effect (eqn (4))

$$\log R = \log_{10}(CFU_{control}) - \log_{10}(CFU_{sample}) \quad (4)$$

2.12. Release of lignin from nanocellulose–lignin films into food simulants

Two food simulants were used according to the Commission Regulation (EU) No. 10/2011 for plastic materials and articles intended to come into contact with food: (1) simulant A: aqueous solution with 10% ethanol (v/v), simulating foods with hydrophilic character capable of extracting hydrophilic substances; (2) simulant D1: aqueous solution with 50% ethanol (v/v), simulating lipophilic foods capable of extracting lipophilic substances, such as alcoholic substances and oil : water emulsions. A piece of each film (around 20 mg) was immersed in 10 mL of the food simulant, and kept in a thermostatic bath at 40 °C for 10 days. Aliquots of 100 μL were taken periodically from the release medium, and the total phenolic content of these aliquots was determined following the Folin–Ciocalteu method with some variations.[20] In brief, a mixture consisting of 100 μL of sample, 500 μL of 1 : 10 Folin–Ciocalteu reagent : water, and 400 μL of 7.5% (w/v) Na_2CO_3 solution was incubated at 50 °C for 10 min. After cooling, absorbance at 760 nm was measured using a Lambda 365 UV-vis spectrometer (PerkinElmer, USA). Gallic acid was used for preparing a calibration curve and the results were expressed as mg of gallic acid equivalents (GAE) per mg of film.

3. Results and discussion

3.1. Nanocellulose–lignin film characterization

Two different protocols were used to prepare nanocellulose–lignin films, differing in how lignin was added to the nanocellulose suspension before film formation: one method involved adding bulk lignin to the suspension (CNF-L), while the other promoted the *in situ* formation of lignin nanoparticles (CNF-LNP). As can be observed in Fig. 1, both methods provided homogeneous and transparent films that became increasingly brown with rising lignin content (color will be discussed in more detail in Section 3.5). The thickness and bulk density of the films are shown in Fig. 2. It was observed that the thickness of the nanocellulose films (35.9 ± 0.8 μm) was reduced when incorporating bulk lignin (29.3 ± 1.0 μm, 28.9 ± 1.3 μm and 31.3 ± 1.4 μm for CNF-2.5L, CNF-5L and CNF-10L, respectively), probably due to a good interaction between lignin and nanocellulose, allowing the filling of gaps between the cellulose nanofibers. Similarly, Wang *et al.*[21] observed an

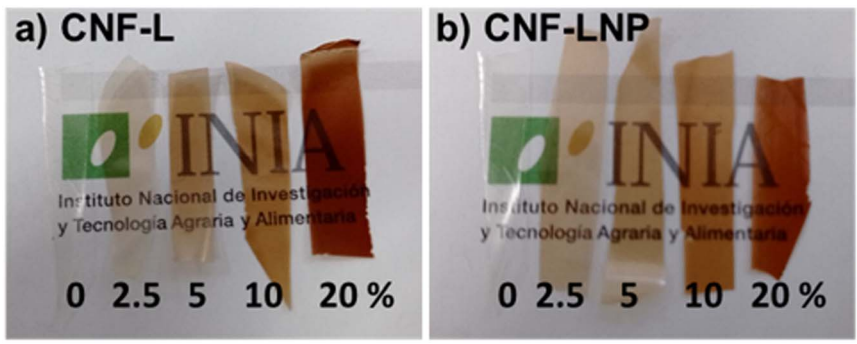

Fig. 1 Nanocellulose–lignin films with bulk lignin (a) and lignin nanoparticles (b). The lignin content of each film is indicated in the bottom of the images.

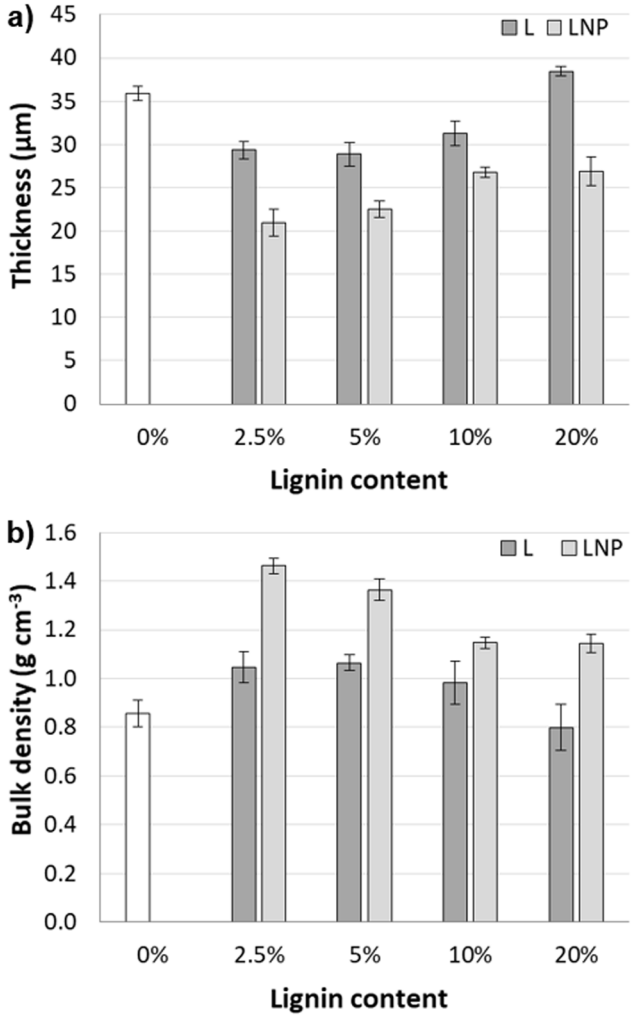

Fig. 2 Thickness (a) and bulk density (b) of nanocellulose–lignin films.

increase in bulk density from 0.83 to 0.93 g cm^{-3} when lignin was incorporated into CNF films, similar to that found in this work: from 0.96 g cm^{-3} for CNF films to 0.98–1.06 g cm^{-3} for CNF-L films with up to 10% lignin content. Furthermore, Liu *et al.*,[22] Pasquier *et al.*[18] and Kim *et al.*[23] reported that the addition of lignin can improve the colloidal stability and dispersion of CNFs, due to electrostatic repulsion between both types of negatively charged particles/fibers, which can prevent coalescence during film formation and agglomeration of CNFs during the drying process. This fact can increase the density of the films and the final mechanical properties and also allow a fast redispersion of the composite films.[22,23] However, when 20% bulk lignin was incorporated, an increase in thickness and reduction in bulk density was found (CNF-20L: 38.4 $\pm$ 0.5 μm and 0.80 g cm^{-3}), likely due to aggregation of lignin, which can deposit on the surface of the CNFs, increasing the space between the CNFs and interfering with the intermolecular hydrogen bonds between nanofibers.[24]

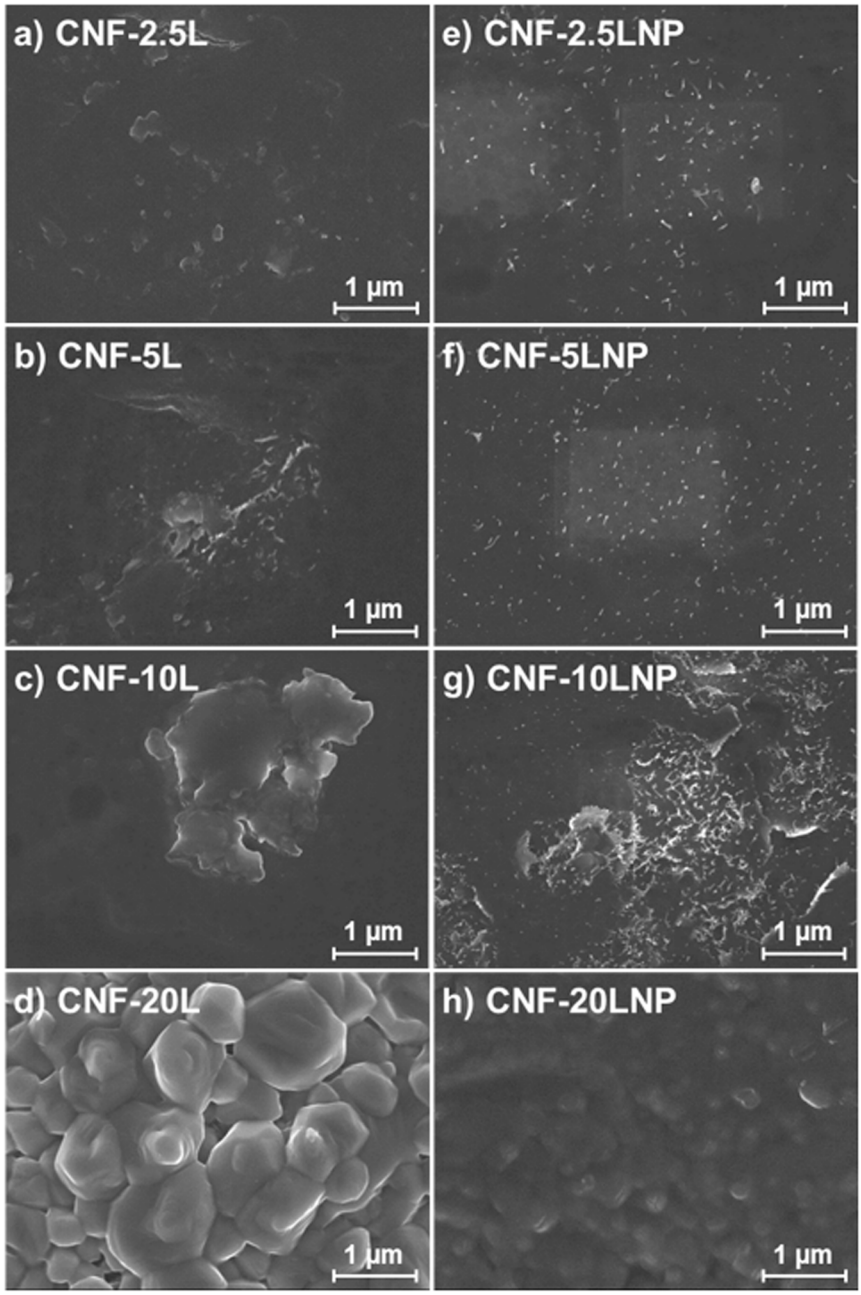

Fig. 3 SEM images of the surfaces of the nanocellulose–lignin films at a magnification of ×23 000.

When lignin nanoparticles were formed in the nanocellulose suspension, the resulting films showed a greater reduction in film thickness (21.0 ± 1.5 μm, 22.5 ± 0.6 μm, 26.8 ± 0.8 μm and 26.9 ± 1.7 μm for CNF-2.5LNP, CNF-5LNP, CNF-10LNP and CNF-20LNP, respectively). The smaller size of the lignin

nanoparticles and the absence of lignin aggregates allowed not only better interaction at the nanometric scale between the LNPs and cellulose nanofibers,[16] but also the filling of smaller spaces between the nanofibers, even for 20% lignin addition, since no LNP aggregates were found (Fig. 3), as it will be mentioned below. Thus, the formation of *in situ* LNPs achieved higher packing and higher bulk density of the final material (1.15–1.46 *vs.* 0.80–1.06 g cm^{-3} for CNF-LNP and CNF-L films, respectively). Similarly, Wang *et al.*[25] reported an increase in bulk density from 1.10 to 1.17–1.25 g cm^{-3} when comparing CNF films with those with 15% LNPs.

The surface morphology of the nanocellulose–lignin films was studied *via* SEM (Fig. 3). As can be observed, irregular lignin particles were found in films with bulk lignin increasing the size of these particles when increasing the lignin content. Thus, CNF-20L films showed lignin aggregates of different sizes up to more than 1 μm, which caused the increase in film thickness, as mentioned above. On the other hand, when lignin was added dissolved in acetone : water, lignin nanoparticles were formed, with smaller particles being observed in the surface of the film. When the lignin content increased, bigger nanoparticles were formed, in agreement with results found for lignin nanoparticle formation by solvent shifting in the absence of cellulose nanofibers.[26] Thus, CNF-20LNP showed spherical LNPs of around 200–400 nm.

Films were characterized *via* FTIR spectroscopy, and spectra in the 4000–600 cm^{-1} range can be found in the ESI (Fig. S.1†). Fig. 4 shows the 1800–600 cm^{-1} region of these spectra, where the most characteristic bands can be found. All the films clearly showed the typical bands for cellulose rings (C–O–C) at 1160, 1105, 1051 and 1025 cm^{-1}.[27] The band at 1600 cm^{-1}, associated with C═O vibrations in –COONa groups, and at 1410 cm^{-1}, associated with C–O symmetric stretching of dissociated carboxyl groups, confirmed the oxidation of the hydroxyl group at C6 of cellulose during the TEMPO-mediated oxidation pretreatment in the preparation of the cellulose nanofibers.[28] This correlates with the high carboxyl content determined *via* conductimetric titration (1043 ± 150 μmol g^{-1}). When lignin was incorporated into the films, either in the form of bulk lignin or LNPs, some of the typical bands associated with lignin were also observed, increasing in intensity when the lignin content increased. Nevertheless, other lignin bands were not found due to overlap with cellulose signals. Thus, only two of the three bands associated with aromatic ring vibrations (1515 and 1420 cm^{-1}) were observed, being the aromatic ring band at 1610 overlapped with that of the carboxylate groups in cellulose at 1600 cm^{-1}. Other observed lignin signals were associated with C–H asymmetric vibrations and deformations (1455 cm^{-1}) and with guaiacyl (1270 and 1216 cm^{-1}) and syringyl units (835 cm^{-1}), both typical units from hardwood materials such as eucalypt. Interestingly, lignin signals were more prominent in films with LNPs compared to those with bulk lignin (comparing samples with similar lignin content).

The thermal stability of the nanocellulose–lignin films was studied *via* TGA. The weight *vs.* temperature curves and their first derivatives are shown in Fig. 5, while the corresponding degradation temperatures are shown in Table S.1.† No big changes were found in the two main degradation temperatures of the nanocellulose–lignin films (242 and 296 °C for the CNF film), observing only slight increases, especially for the 10 and 20% lignin contents (243–244 and 297–299 °C for films with 10–20% bulk lignin or LNPs). Neither were significant changes

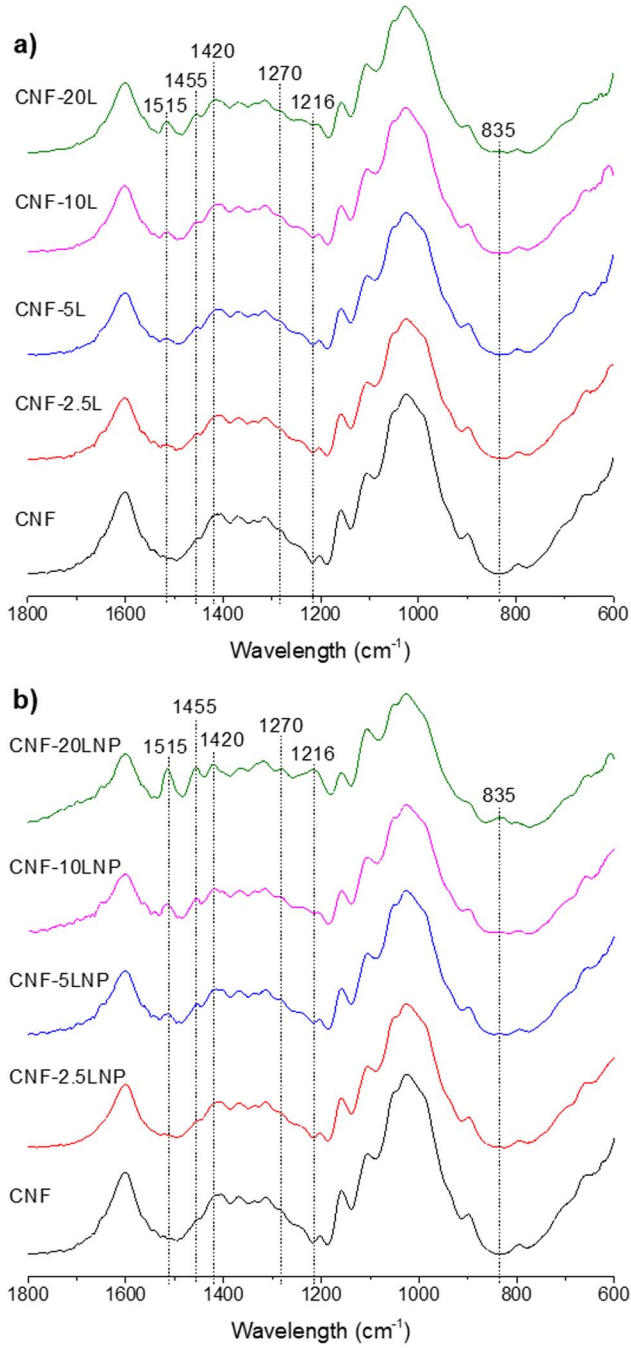

Fig. 4 FTIR spectra of nanocellulose–lignin films in the 1800–600 cm^{-1} range: (a) films with bulk lignin and (b) films with LNPs.

found in the temperature at which 5% weight loss occurred, with only a slight reduction from 228 °C to 226–227 °C being observed for films with 2.5–10% L or 2.5–5% LNPs. Controversial results have been reported about the influence of

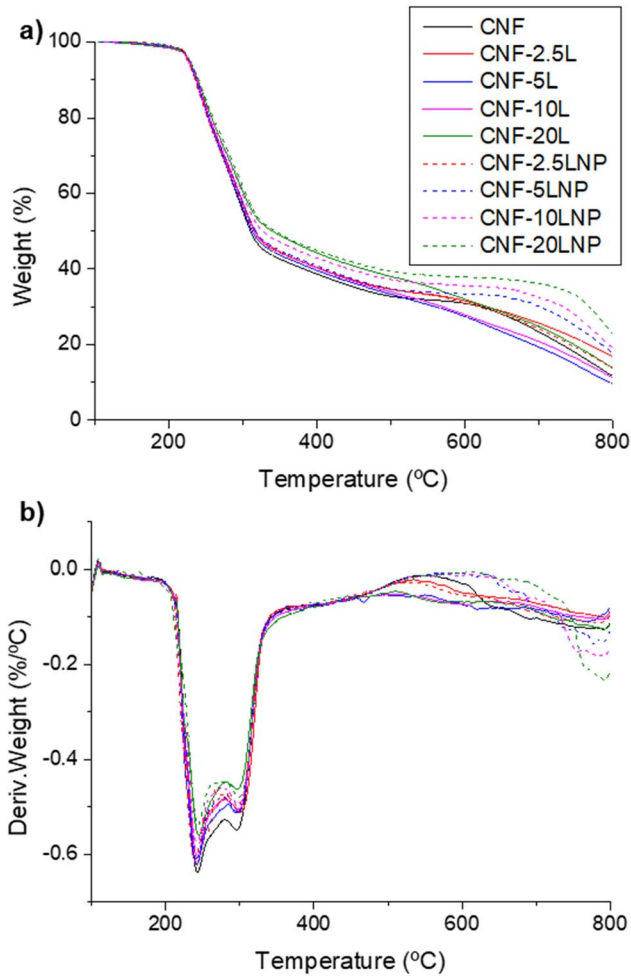

Fig. 5 TGA curves: (a) weight loss and (b) its first derivative *versus* temperature of nanocellulose–lignin films.

lignin/LNP incorporation on the thermal stability of CNF films. Some authors have reported no significant changes in the thermal properties of CNF films when incorporating small amounts of lignin or LNP (0.5–25%),[22,29] in spite of the higher thermal stability of lignin compared to CNFs, while other authors have described improvements in thermal stability when incorporating 5% different kraft lignins[30] or 5% lignin nanoparticles.[31] It is interesting to point out that when lignin nanoparticles were formed, a delay in weight loss at 600–800 °C (associated with higher T_{off} in nanocellulose–lignin films with 5–20% LNPs) was found, which could be related to slightly improved thermal stability. This finding could indicate a better interaction between nanocellulose and lignin when the latter is in the form of nanoparticles, probably due to the higher available surface area of LNPs and the absence of lignin aggregates. Similarly, Nair *et al.*[32] reported enhanced thermal stability for PVA–LNP composite films compared to a PVA–lignin composite. These authors attributed it to a good dispersion of LNPs into the PVA

matrix with lower agglomeration than in the case of bulk lignin, resulting in a better miscibility of both components and stronger intermolecular hydrogen bonds between them.

3.2. Water solubility and swelling capacity of nanocellulose–lignin films

The stability of the nanocellulose–lignin films in water was analyzed by determining both their water solubility and swelling capacity (Fig. 6). Note that the incorporation of bulk lignin into the film progressively increased their solubility from 20.5% ± 2.9% for the nanocellulose film without lignin (CNF) to 32.4 ± 1.2% for the film with 20% bulk lignin (CNF-20L), while only a slight increase was observed due to the incorporation of LNPs (24.7 ± 2.2% for CNF-20LNP). These data may indicate that the incorporation of LNPs does not reduce the bonding strength between cellulose nanofibers, while the presence of lignin aggregates weakens the cellulose web, in line with what was found for the thermal stability. Wang *et al.*[25] also suggested that the presence of large lignin aggregates, due to

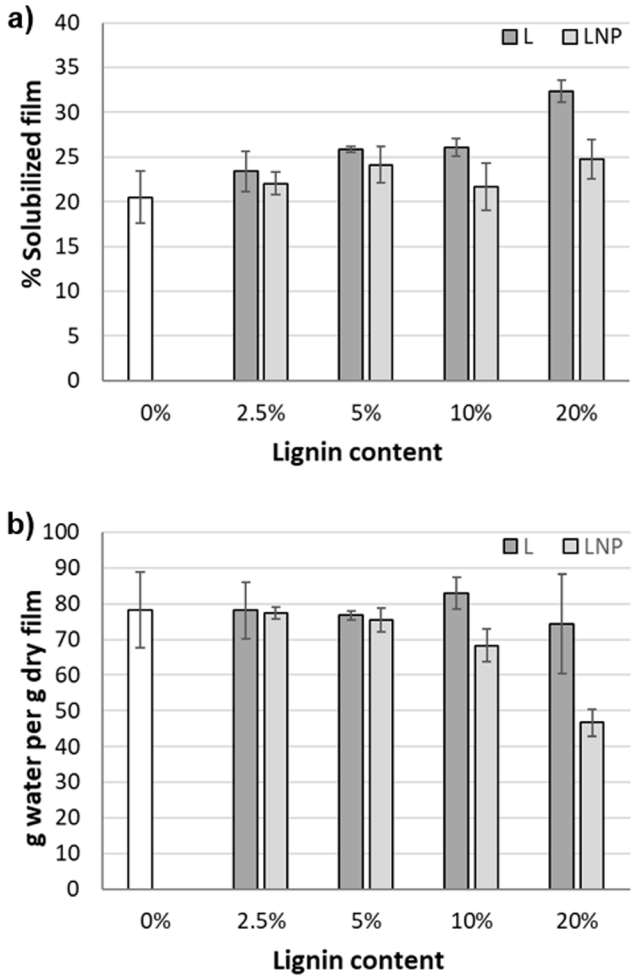

Fig. 6 Solubility (a) and swelling capacity (b) of nanocellulose–lignin films.

the incorporation of a high amount of lignin (such as 20%), hinders the hydrogen bonding between cellulose microfibers.

On the other hand, the swelling capacity of the films with bulk lignin did not significantly change compared to the CNF film (78 ± 10 *vs.* 74–83 g of water per g of dry film), in spite of the relative reduction of cellulose amount in the films. The reason could be that the presence of lignin aggregates introduces more space between cellulose nanofibers, acting as nano- or micro-spacers,[33] and this new space could be occupied by a higher amount of water. In contrast, when LNPs were incorporated into the film, lower swelling capacity was found, with a linear correlation being observed between swelling and LNP content, especially for LNP contents between 5% and 20% (*R*-squared of 0.9922). As mentioned above, the incorporation of LNPs did not significantly reduce the bonding between cellulose nanofibers, nor incorporate significant spaces between nanofibers, the small size of the nanoparticles being the key to avoid the disruption of the strong fibrillar network.[18] However, due to the incorporation of lignin, the amount of cellulose in the film is reduced, also reducing the hygroscopicity of the film and the available surface for water adsorption. A similar effect in water absorption capacity (or swelling capacity) was found by Agustin *et al.*[34] when they incorporated LNPs into nanocellulose cryogels.

3.3. Water vapor permeability of nanocellulose–lignin films

Water vapor permeability (WVP) was evaluated by measuring the water vapor transmission rate of each film at 75% relative humidity and 23 °C (Fig. 7a). All the films showed WVPs of 9.7–20.5 × 10^{-11} g m^{-1} s^{-1} Pa^{-1}, only slightly higher than those reported for different bioplastics such as polylactic acid (PLA),

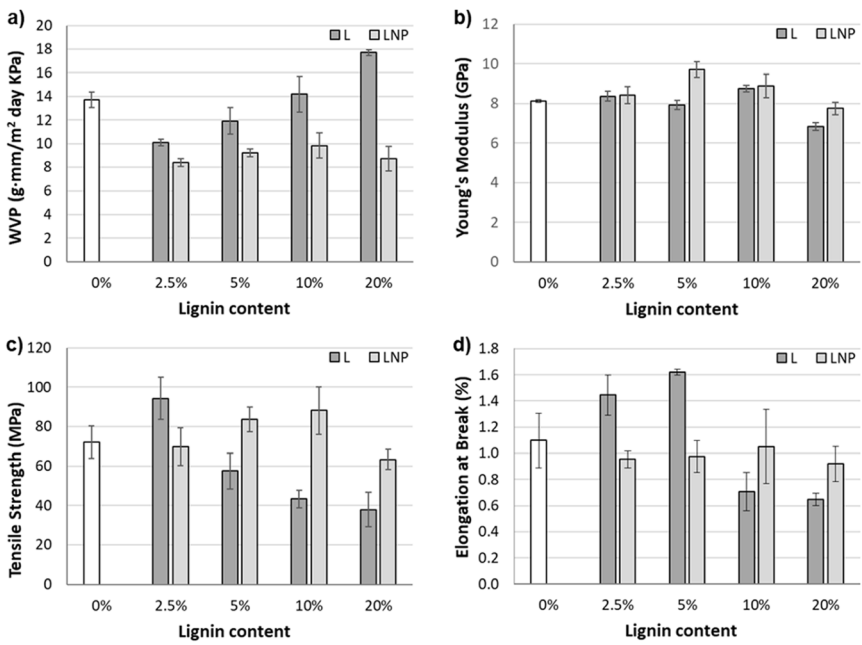

Fig. 7 Barrier and mechanical properties of nanocellulose–lignin films: (a) water vapor permeability; (b) Young's modulus; (c) tensile strength; and (d) elongation at break.

polyhydroxybutyrate (PHB) or hydroxypropyl methylcellulose (HPMC): 1.9–17.9 × 10^{-11} g m^{-1} s^{-1} Pa^{-1}.[6,35,36] Furthermore, it should be taken into account that the WVP highly depended on the conditions during the test, and also on the procedure followed for the film preparation. Thus, the WVP could be improved by forming the films *via* filtration and hot-pressing instead of casting.[37,38] Nevertheless, these WVP values for bioplastics are significantly higher than those corresponding to traditional plastics such as high-density polyethylene (HDPE, 1.7–3.5 × 10^{-14} g m^{-1} s^{-1} Pa^{-1}), low-density polyethylene (LDPE, 6.7–8.7 × 10^{-14} g m^{-1} s^{-1} Pa^{-1}), polypropylene (PP, 2.3–4.6 × 10^{-14} g m^{-1} s^{-1} Pa^{-1}) or polystyrene (PS, 11.3–45.5 × 10^{-14} g m^{-1} s^{-1} Pa^{-1}).[39]

When a low percentage of lignin (2.5%) was incorporated into the nanocellulose film, an improvement in barrier properties was observed with both LNPs and bulk lignin. This effect has been associated with LNPs/lignin filling the voids between cellulose nanofibers[16,25] or with strong intermolecular interactions between lignin and different biopolymer matrixes (such as HPMC, PLA, agar or chitosan).[6,13,40,41] In the case of LNPs, the decrease in WVP was bigger, due to the smaller size of the LNPs compared to bulk lignin.[30] Furthermore, no significant changes were observed when the LNP content increased from 2.5% to 20%. However, when bulk lignin was added, a progressive increase in WVP was observed when increasing the lignin content, probably due to lignin aggregation (observed *via* SEM, Fig. 3), which increased the spaces between the nanofibers and weakened the cellulose web, as mentioned above. In contrast, due to their reduced size, LNPs did not cause a disruption of the cellulose nanofibrils, in line with what was observed for the water solubility and swelling capacity of the films. Furthermore, thermal stability also indicated better interactions between nanocellulose and lignin when lignin was in form of nanoparticles, contributing to preventing the decay of barrier properties.

3.4. Mechanical properties of nanocellulose–lignin films

The mechanical properties of the films were measured *via* tensile tests. Young's modulus, tensile strength and elongation at break (Fig. 7b–d) were calculated from the strength *vs.* elongation curves for each type of film. In general, it was observed that the addition of lignin did not significantly change these mechanical properties compared to the CNF films without lignin, especially when it was added allowing the formation of LNPs. Nevertheless, reductions in the tensile strength (Fig. 7c) and elongation at break (Fig. 7d) values were found when bulk lignin was added in equal or higher percentages than 10%, due to the presence of lignin aggregates (from 72 MPa to 43–38 MPa and from 1.1% to 0.7–0.6%, respectively), while increases in both properties were observed when bulk lignin was added in low amounts (up to 94 MPa and 1.4% for CNF-2.5L films). A similar effect has been previously reported by several authors,[6,16,17,42–44] who described a plasticizing effect when lignin was added to different polymers in small amounts, but which turns into a drop in mechanical properties when lignin is added in excess due to lignin aggregation (clearly observed in CNF-10L and CNF-20L (Fig. 3c and d)). However, these effects were not so clear when lignin was added in the form of LNPs, with smaller increases in tensile strength and Young's modulus being observed for CNF-5LNP and CNF-10LNP and decreases for CNF-20LNP compared to CNF films. The lesser effect of the addition of LNPs could

be due to the smaller size of these nanoparticles, which did not significantly disturb the cellulose nanofibril net,[18] as mentioned above. Similar results were found by Inoue *et al.*,[45] who observed a significant reduction in mechanical properties when 10% bulk lignin was added to CNF films, while the addition of 10% LNPs caused much lower decreases.

In conclusion, the resulting CNF-LNP films showed higher tensile strength and Young's modulus compared to other biopolymers proposed for packaging (tensile strength of 63–88 MPa *vs.* 15–35 MPa for PHB, 28–57 MPa for PLA or 6.4–43 MPa for polyvinyl alcohol (PVA) and Young's modulus of 7.7–9.7 GPa *vs.* 1.2–2.2 GPa for PHB, 1.8–2.8 GPa for PLA or 1.2–2.1 GPa for PVA),[35,36,46–50] even higher than those of other traditional plastics (tensile strength of 7–25 MPa for LDPE, 19–31 MPa for HDPE, 31–49 MPa for PS or 42–55 MPa for polyvinyl chloride (PVC) and Young's modulus of 0.15–0.34 GPa for LDPE, 0.8–0.9 GPa for HDPE, 2.7–3.4 GPa for PS or 2.8 GPa for PVC).[39] However, the elongation at break was much lower than that reported for those polymers (0.9–1.1% *vs.* 2–10% for PHB, 4.8–25% PLA, 80–400% for PVA, 300–900% for LDPE, 20–50% for HDPE, 2–3% for PS or 20–180% for PVC).[35,36,39,46–50] Nevertheless, the elongation at break could be increased by adding a plasticizer to the films.

3.5. Optical properties and UV-shielding capacity of nanocellulose–lignin films

The optical properties of the films were evaluated by measuring the transmittance between 200 and 800 nm and the CIE $L^*a^*b^*$ color coordinates. The total transmittance *vs.* wavelength curves are shown in Fig. 8. A clear reduction in transparency (indicated by the total transmittance at 600 nm) was found when increasing the lignin content (either as bulk lignin or LNPs), as was expected: 89.7% for pure CNF, 81.0–80.8% for 2.5% lignin, 74.1% for 5% lignin, 62.7–63.5% for 10% lignin and 42.9% for 20% lignin. Nevertheless, these values of

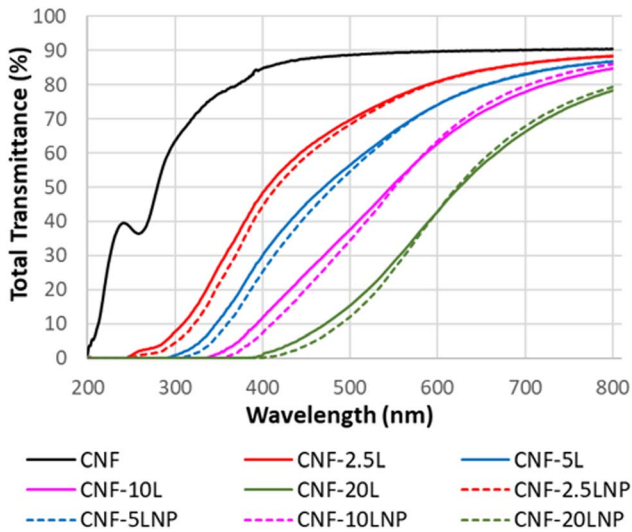

Fig. 8 Total transmittance *vs.* wavelength curves for nanocellulose–lignin films, from 200 to 800 nm.

Table 1 CIE $L^*a^*b^*$ color coordinates of the bionanocomposite films, color changes (ΔE) compared to an HPMC film, and opacity and transmission haze at 600 nm

Sample	L^*	a^*	b^*	ΔE	Opacity (u.a. mm^{-1})	Transmission haze (%)
CNF	95.0 ± 0.8	−0.5 ± 0.0	4.1 ± 0.3	—	1.3 ± 0.6	9.2 ± 0.2
CNF-2.5L	84.4 ± 1.0	1.1 ± 0.3	20.5 ± 1.4	19.6 ± 1.7	3.1 ± 0.8	16.8 ± 0.4
CNF-5L	73.3 ± 0.8	5.7 ± 0.3	34.6 ± 0.7	38.0 ± 1.1	4.5 ± 1.1	22.4 ± 0.6
CNF-10L	59.6 ± 1.1	13.3 ± 0.6	43.1 ± 1.1	54.5 ± 1.7	6.5 ± 0.9	32.4 ± 0.1
CNF-20L	43.0 ± 1.4	20.4 ± 0.5	32.1 ± 1.0	62.7 ± 1.8	9.6 ± 1.3	42.3 ± 0.8
CNF-2.5LNP	82.8 ± 0.6	1.6 ± 0.2	25.2 ± 0.8	24.5 ± 1.0	4.4 ± 0.6	14.5 ± 0.8
CNF-5LNP	75.0 ± 0.7	5.1 ± 0.4	37.3 ± 0.9	39.2 ± 1.2	5.8 ± 0.8	13.8 ± 0.9
CNF-10LNP	59.8 ± 0.3	15.3 ± 0.5	49.8 ± 0.1	59.9 ± 0.6	6.4 ± 0.7	11.3 ± 0.5
CNF-20LNP	40.1 ± 0.6	25.3 ± 0.2	34.1 ± 1.5	67.7 ± 1.7	13.7 ± 0.9	25.0 ± 0.7

transmittance allow seeing through the films, even those with 20% lignin content (Fig. 1). Similar results have been found previously for nanocellulose films containing lignin or LNPs, due to the dark brown color of lignin.[29,31,44] No significant differences in total transmittance at 600 nm were found between films with bulk lignin or LNPs. Nevertheless, when opacity was calculated taking into account the thickness of the films (Table 1), slightly higher values of opacity were found for LNP-containing films (comparing films with the same lignin content). This fact is due to the lower thickness of the LNP-containing films, as mentioned in Section 3.1, originating from the smaller size of the LNPs and the absence of lignin aggregates. Furthermore, the presence of lignin aggregates in the CNF-L films caused higher increases in transmission haze at 600 nm, especially when increasing the lignin content. This parameter indicates the amount of light that deviates from the incident beam by more than 2.5° when it passes through the film. Thus, the larger the size and amount of lignin aggregates, the greater the amount of light deviating due to light scattering, therefore resulting in a greater transmission haze.

Fig. 8 also showed great UV-blocking due to the presence of lignin in the films. The higher the amount of lignin, the higher the UV-blocking effect, as previously reported.[15,18,29,31,44] This effect is due to lignin's aromatic functional groups, such as phenolic and conjugated carbonyl groups.[15,18,29,31,44,51] Thus, 20% lignin was required to completely block UV under 400 nm; however, a film with only 5% lignin completely blocked UV-B (315–280 nm), the most energetic component of natural UV light. Comparing bulk lignin with LNPs, higher UV-blocking was found for LNP-containing films (for a fixed lignin content). The self-assembly of lignin to form the nanoparticles caused the confinement of π–π aromatic aggregates, enhancing the UV-blocking properties.[15,29,51]

CIE $L^*a^*b^*$ color coordinates were also evaluated to determine the color change (ΔE) of the films due to the addition of lignin when comparing them to the CNF film (Table 1). The lightness of the films (L^* coordinate) was significantly reduced when increasing the lignin content, as was expected due to the dark color of lignin. Furthermore, clear increases in positive values of both the a^* coordinate (indicating red color) and the b^* coordinate (indicating yellow color) were observed when increasing lignin content. The only exception was the reduction in the b^* coordinate when increasing the lignin content from 10% to 20%.

Nevertheless, the global color change (ΔE) indicated an increase in color due to the increase in lignin content, even in the latter samples. Interestingly, film samples with LNPs showed greater color changes than those containing bulk lignin. As mentioned above, higher UV-blocking was associated with LNPs, which has been previously related to a darker color.[31]

3.6. Antioxidant capacity of nanocellulose–lignin films

Antioxidant capacity is a desirable property for several applications, such as food packaging, since it contributes to protection of food against oxidation, reducing flavour loss, nutrient decomposition and production of toxic compounds.[52] The incorporation of lignin or LNPs into nanocellulose or other non-antioxidant polymer films provides films with antioxidant capacity, as previously demonstrated by several authors.[6,17,18,53–56] The ability of lignin to stop the propagation of oxidation reactions is related to the scavenging of free radicals by hydroxyl phenolic groups, but also to the presence of methoxy groups, conjugated double bonds and π structures, which stabilize phenoxy radicals *via* resonance.[57] Thus, Fig. 9a shows the antioxidant capacity of films with different lignin contents, showing a clear increase in antioxidant capacity when increasing the lignin content. Nevertheless, a linear correlation between lignin content and antioxidant capacity was not always found in insoluble films such as the ones developed in this work, which indicated that the antioxidant activity can be related to surface activity and not only to migration of active compounds from the film.[17,18,54,58]

Meanwhile, films containing lignin nanoparticles (LNPs) exhibited higher antioxidant capacity compared to those incorporating bulk lignin. The only exception was films with 2.5% lignin content, which showed similar antioxidant activity. However, when lignin content increased, bulk lignin started forming aggregates in the film, which can hide active groups, resulting in lower antioxidant activity.[54] Furthermore, as other authors have previously reported, the formation of LNPs increased the antioxidant activity due to the higher surface area of LNPs compared to bulk lignin and lignin aggregates, which increases the accessibility to surface active functional groups.[17,18,29]

3.7. Antibacterial capacity of nanocellulose–lignin films

The use of materials able to control bacterial growth is very interesting in several applications, including medical and food packaging. Although nanocellulose does not have antibacterial properties, the introduction of lignin or LNPs into the nanocellulose matrix would confer antibacterial capacity to the resulting films. Thus, the antibacterial capacity of CNF-L and CNF-LNP films was tested against Gram-positive and Gram-negative bacteria: *S. aureus* and *E. coli*, respectively (Fig. 9b and c), both selected due to their association with human infections and food spoilage.[59,60] A significant growth inhibition was found for both bacteria, especially *S. aureus*, reaching $\log R$ values between 3.3 and 7.2, which means inhibition in bacterial growth from 99.95% to 99.99998%, depending on the lignin content and on the protocol followed for the preparation of the films. The higher antibacterial effect against *S. aureus* could be related to the lack of cell membrane and the interaction of lignin with the dense peptidoglycan layer of Gram-positive bacteria.[11,42,61] In agreement, other authors have reported a higher antibacterial effect of lignin against *S. aureus* compared to *E. coli*.[62,63]

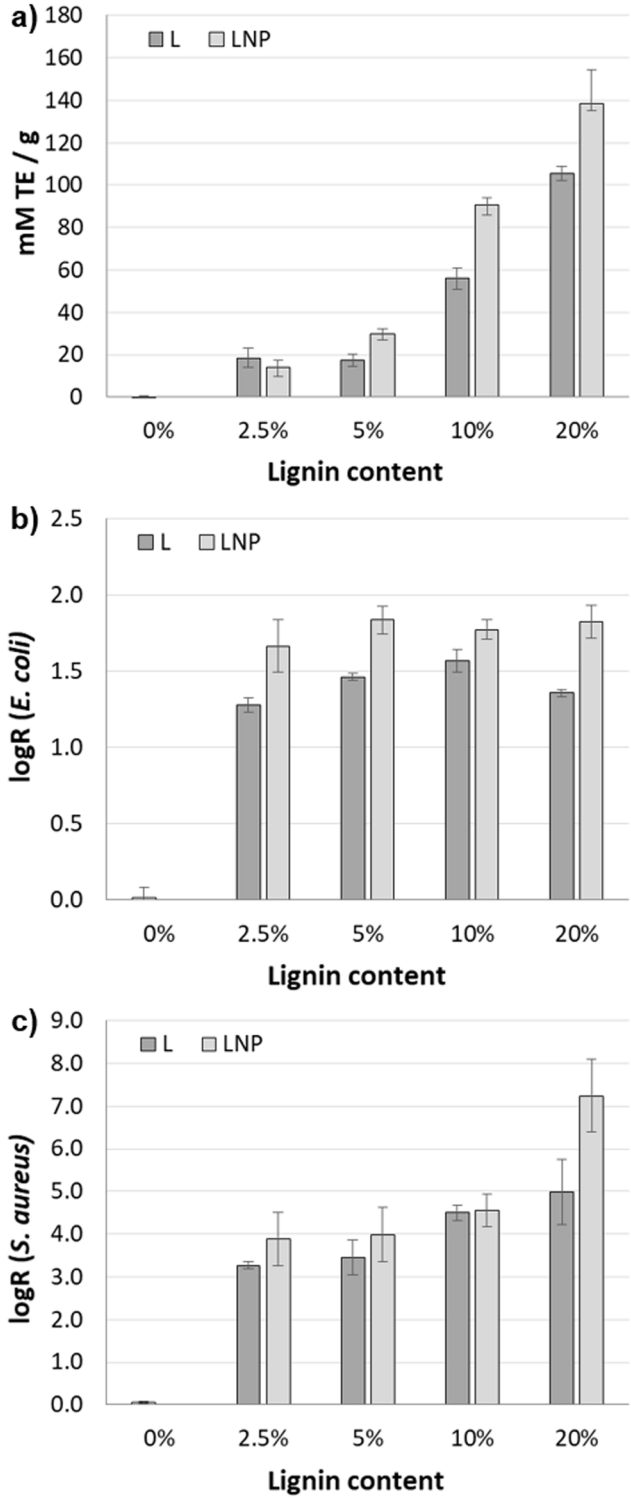

Fig. 9 Active properties of nanocellulose–lignin films: (a) antioxidant capacity, (b) antibacterial capacity against *E. coli* and (c) antibacterial capacity against *S. aureus*.

Although the antibacterial mechanism of lignin is not clear, it is normally ascribed to rupture of cell membranes and to accumulation of reactive oxygen species (ROS) on the bacterial surface,[64,65] which causes oxidative stress and therefore growth inhibition. Moreover, this ROS antibacterial mechanism is normally related to the antioxidant capacity of lignin.[64] Thus, its phenolic structure allows lignin to penetrate the cell wall *via* hydroxyl–lipid interactions, resulting in damage of the cell membrane and subsequent rupture of bacterial components.[65] Therefore, antibacterial capacity is directly related to hydroxyl phenolic content, but also to the methoxy groups, methyl group on C_γ or side chains with $C_\alpha{=}C_\beta$.[11,12,29,62,66] Moreover, lignin nanoparticles exhibit a notable affinity for bacterial surfaces, enabling the nanoparticles to attach to bacterial membranes and to interact with proteins and lipids, causing membrane disruption and inhibition of the respiratory chain, plus oxidative damage, which impedes bacterial proliferation.[65,67] These phenomena explain the higher antibacterial effect found when lignin content increased, and also when LNPs were present in the film instead of bulk lignin. Moreover, the tiny size of LNPs may trigger the formation of adenosine triphosphate (ATP) due to lignin introduction inside the bacteria and acidification of the medium due to its weakly acidic groups. In addition, LNPs may affect protein synthesis in ribosomes, blocking normal bacterial metabolism and leading to bacteria death.[68,69]

3.8. Release of lignin from nanocellulose–lignin films into food simulants

As mentioned above, the antioxidant and antibacterial activity of insoluble films can be related both to surface activity and to migration of active compounds from the film. To study the migration of lignin from the films, two food simulants were used and the release of phenols was quantified (Fig. 10). It was observed that the release of lignin or LNPs (directly related to the release of phenols) took place mainly in the first 30 min of immersion, and increased with the lignin/LNP content of the films, as expected. Only in the films with 20% lignin/LNPs did migration of phenol continue during the subsequent hours, but it stopped after 24 hours, with the phenol concentration in the supernatants remaining

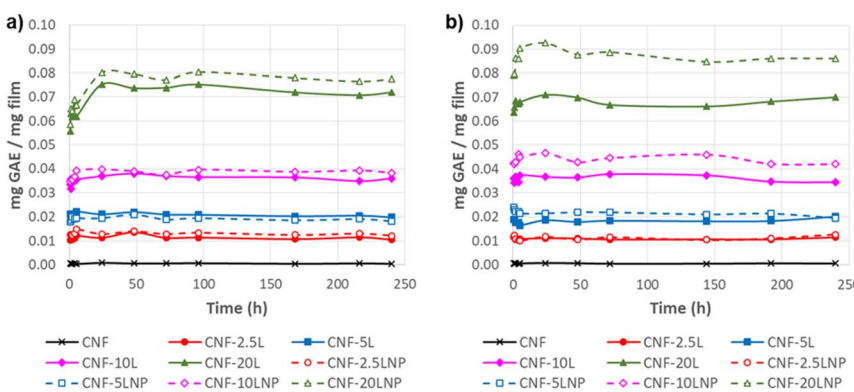

Fig. 10 Release of phenols (directly related to release of lignin) when films were immersed for 10 days at 40 °C in (a) aqueous solution with 10% ethanol or (b) aqueous solution with 50% ethanol.

unchanged after this time. Comparing films with similar lignin contents but formed following the two different proposed protocols (bulk lignin or LNP formation), similar lignin releases were found using simulant A (10% ethanol), corresponding to 66–73% of the initial lignin content of each film. However, significant differences were found with simulant D1 (50% ethanol), with a higher release observed when lignin was in form of LNPs, especially for lignin contents higher than 5%. Thus, the release of lignin, comparing LNPs *vs.* bulk lignin, was 67 *vs.* 77%, 66 *vs.* 80% and 64 *vs.* 79% for 5%, 10% and 20% lignin contents, respectively. This higher release was likely due to the smaller size of LNPs compared to lignin aggregates, which makes their dissolution in food simulants and/or their migration/diffusion through the CNF film easy.

Comparison with lignin-containing traditional plastics or bioplastics is hard to establish, not only due to lack of data, but also due to different experimental methods and conditions of the migration/release assays. For example, Mikulášová and Košíková[70] studied the release of lignin from lignin–PP composite films, and observed a clear release of lignin when immersed in culture medium. However, they use culture medium instead of food simulant with ethanol and carried out the assays at lower temperature, which can explain the lower release of lignin compared to that observed in our work, masking the real effect of using PP instead of nanocellulose as a matrix. Another example, using phenols instead of lignin, is that reported by Peltzer *et al.*,[71] who studied the release of carvacrol (a natural phenol compound) from HDPE and observed lower release than in our study. Nevertheless, they used different food simulants (olive oil or water) and the behavior of carvacrol is not comparable to that of lignin. When the release of lignin from bioplastics was studied instead of that from traditional plastics, a comparison was also hard to establish. Thus, Pasquier *et al.*,[18] who studied the release of lignin nanoparticles from lignin–cellulose nanofiber or lignin–chitosan fiber films, observed lower release of lignin (<5%) compared to our results. However, this lower release is probably due to the conditions chosen for the release assay: (1) they used water instead of a food simulant containing ethanol (10% in food simulant A and 50% in food simulant D1), so the solubility of lignin was significantly lower; (2) they carried out the assay at room temperature instead of 40 °C, which can also reduce the solubility of lignin, since migration is directly dependent on temperature according to the Arrhenius equation; (3) they carried out the assay for 1 hour instead of 10 days, limiting the liberation time. Nevertheless, their lower release of LNPs could be also due to better interaction between lignin and the nanofibers, especially the chitin nanofibers with a positive charge (and LNPs with a negative charge).

Finally, considering the results found for lignin release in our nanocellulose–lignin films, the antibacterial capacity of the films against *S. aureus* seems to be related to the migration of phenols from the films: similar antibacterial capacities for films with the same lignin contents (independently of the presence of bulk lignin or LNPs), except for CNF-20LNP in which there was higher release of phenols compared to CNF-20L, could explain the higher antibacterial capacity. However, the antibacterial capacity against *E. coli*, as well as the antioxidant capacity of the films, seems to be more related to the surface activity of the films, which was enhanced in films with LNPs due to the greater accessibility of active functional groups on the surface of LNPs compared to bulk lignin and lignin aggregates.[17,18,29]

4. Conclusions

The incorporation of lignin into cellulose nanofiber films gave them active properties, regardless of whether the lignin was added in bulk form or as lignin nanoparticles (LNPs). However, when lignin was incorporated into the nanocellulose suspension, allowing the *in situ* formation of LNPs, the resulting films showed higher antioxidant, antibacterial and UV-shielding properties compared to those obtained with bulk lignin. Moreover, improvements in water vapor permeability and mechanical properties were also displayed, even for a 10–20% LNP content. Consequently, CNF–LNP films exhibited excellent barrier, mechanical and bioactive properties compared with other bioplastics, making them promising candidates for active food packaging applications. Compared with traditional plastics, good mechanical properties were achieved, but greater improvements in barrier properties are still needed. However, compared to the most commonly used protocols for preparing CNF-LNP films (involving a first step for the formation of LNPs and a second step for their incorporation into the nanocellulose suspension), the protocol proposed in this work simplifies the process to one step, making it easier to industrially scale up.

Data availability

The main data related to the results and discussion of this work are present in this article or in ESI.† Primary data or any other data associated with this study are available on request from the corresponding author.

Author contributions

Raquel Martín-Sampedro: conceptualization, investigation, formal analysis, methodology, writing – original draft. Antonio Ovejero-Pérez: investigation, methodology, writing – review & editing. Mercedes Oliet: writing – review & editing, project administration. Virginia Alonso: writing – review & editing. Francisco Rodríguez: writing – review & editing, project administration, funding acquisition. David Ibarra: conceptualization, writing – review & editing, supervision, project administration, funding acquisition. María E. Eugenio: conceptualization, writing – review & editing, supervision, project administration, funding acquisition.

Conflicts of interest

There are no conflicts to declare.

Acknowledgements

This work was supported by the MICIN/AEI/10.13039/501100011033 (Spain) and "ERDF A way of making Europe" [PID2022-141965OB-C21]; the MCIN/AEI/10.13039/501100011033 and the "European Union Next Generation EU/PRTR" [TED 2021-132122B-C21]; and the Comunidad de Madrid (Spain) [SUSTEC-CM S2018/EMT-4348 and TEC2024-BIO-27]. The authors are also grateful for the support of the following Interdisciplinary Platforms: Sustainable Plastics towards

a Circular Economy (SusPlast-CSIC), Sustainability and Circular Economy (SosEcoCir-CSIC) and Horizonte Verde (CSIC).

References

1 H.-M. Wang, T.-Q. Yuan, G.-Y. Song and R.-C. Sun, *Green Chem.*, 2021, **23**, 3790–3817.
2 M. Asgher, S. A. Qamar, M. Bilal and H. M. N. Iqbal, *Food Res. Int.*, 2020, **137**, 109625.
3 M. Jonoobi, R. Oladi, Y. Davoudpour, K. Oksman, A. Dufresne, Y. Hamzeh and R. Davoodi, *Cellulose*, 2015, **22**, 935–969.
4 L. Jiménez-López, M. E. Eugenio, D. Ibarra, M. Darder, J. A. Martín and R. Martín-Sampedro, *Polymers*, 2020, **12**, 2450.
5 N. Lavoine, I. Desloges, A. Dufresne and J. Bras, *Carbohydr. Polym.*, 2012, **90**, 735–764.
6 R. Martín-Sampedro, P. Aranda, G. del Real, E. Ruiz-Hitzky and M. Darder, *Nanoscale Adv.*, 2023, **5**, 4107–4123.
7 M. H. Hussin, J. N. Appaturi, N. E. Poh, N. H. A. Latif, N. Brosse, I. Ziegler-Devin, H. Vahabi, F. A. Syamani, W. Fatriasari, N. N. Solihat, A. Karimah, A. H. Iswanto, S. H. Sekeri and M. N. M. Ibrahim, *Int. J. Biol. Macromol.*, 2022, **200**, 303–326.
8 M. E. Eugenio, R. Martín-Sampedro, J. I. Santos, B. Wicklein and D. Ibarra, *Molecules*, 2021, **26**, 3819.
9 M. E. Eugenio, L. García-Fuentevilla, R. Martín-Sampedro, J. I. Santos, B. Wicklein and D. Ibarra, *Wood Sci. Technol.*, 2025, **59**, 4.
10 M. E. Eugenio, R. Martín-Sampedro, J. I. Santos, B. Wicklein, J. A. Martín and D. Ibarra, *Int. J. Biol. Macromol.*, 2021, **181**, 99–111.
11 A. Alzagameem, S. E. Klein, M. Bergs, X. T. Do, I. Korte, S. Dohlen, C. Hüwe, J. Kreyenschmidt, B. Kamm, M. Larkins and M. Schulze, *Polymers*, 2019, **11**, 670.
12 G. Tedeschi, S. Guzman-Puyol, L. Ceseracciu, U. C. Paul, P. Picone, M. Di Carlo, A. Athanassiou and J. A. Heredia-Guerrero, *Biomacromolecules*, 2020, **21**, 910–920.
13 S. Shankar, J.-W. Rhim and K. Won, *Int. J. Biol. Macromol.*, 2018, **107**, 1724–1731.
14 E. Cavallo, X. He, F. Luzi, F. Dominici, P. Cerrutti, C. Bernal, M. L. Foresti, L. Torre and D. Puglia, *Molecules*, 2020, **26**, 126.
15 C. H. M. Camargos, G. Poggi, D. Chelazzi, P. Baglioni and C. A. Rezende, *ACS Appl. Nano Mater.*, 2022, **5**, 13245–13259.
16 L. Guo, M. Li, Q. Xu, L. Jin and Y. Wang, *Int. J. Biol. Macromol.*, 2023, **227**, 365–372.
17 M. Farooq, T. Zou, G. Riviere, M. H. Sipponen and M. Österberg, *Biomacromolecules*, 2019, **20**, 693–704.
18 E. Pasquier, B. D. Mattos, N. Belgacem, J. Bras and O. J. Rojas, *Biomacromolecules*, 2021, **22**, 880–889.
19 R. Re, N. Pellegrini, A. Proteggente, A. Pannala, M. Yang and C. Rice-Evans, *Free Radical Biol. Med.*, 1999, **26**, 1231–1237.
20 L. Jiménez-López, R. Martín-Sampedro, M. E. Eugenio, J. I. Santos, H. Sixto, I. Cañellas and D. Ibarra, *Wood Sci. Technol.*, 2020, **54**, 1617–1643.

21 X. Wang, Q. Xia, S. Jing, C. Li, Q. Chen, B. Chen, Z. Pang, B. Jiang, W. Gan, G. Chen, M. Cui, L. Hu and T. Li, *Small*, 2021, **17**, 2008011.
22 Y. Liu, *ACS Sustainable Chem. Eng.*, 2018, **6**, 5524–5532.
23 J. Kim, J. Bang, Y. Kim, J.-C. Kim, S.-W. Hwang, H. Yeo, I.-G. Choi and H. W. Kwak, *Carbohydr. Polym.*, 2022, **282**, 119122.
24 A. Andrade, J. Nuñez, S. Henríquez-Gallegos, C. Torres, A. Mendez-Miranda, E. Valenzuela-García, G. Albornoz-Palma, I. Ortega-Sanhueza, O. Valerio, L. Montoya and M. Pereira, *Carbohydr. Polym. Technol. Appl.*, 2025, **9**, 100651.
25 L. Wang, L. Tan, L. Hu, X. Wang, R. Koppolu, T. Tirri, B. van Bochove, P. Ihalainen, L. S. Seleenmary Sobhanadhas, J. V. Seppälä, S. Willför, M. Toivakka and C. Xu, *ACS Sustainable Chem. Eng.*, 2021, **9**, 8770–8782.
26 S. Iravani and R. S. Varma, *Green Chem.*, 2020, **22**, 612–636.
27 C. F. Castro-Guerrero and D. G. Gray, *Cellulose*, 2014, **21**, 2567–2577.
28 S. Fujisawa, Y. Okita, H. Fukuzumi, T. Saito and A. Isogai, *Carbohydr. Polym.*, 2011, **84**, 579–583.
29 X. Wang, S. S. Wang, W. Liu, S. S. Wang, L. Zhang, R. Sang, Q. Hou and J. Li, *Carbohydr. Polym.*, 2019, **225**, 115213.
30 I. Pylypchuk, R. Selyanchyn, T. Budnyak, Y. Zhao, M. Lindström, S. Fujikawa and O. Sevastyanova, *Membranes*, 2021, **11**, 204.
31 H. Bian, X. Shu, W. Su, D. Luo, M. Dong, X. Liu, X. Ji and H. Dai, *Int. J. Mol. Sci.*, 2022, **23**, 14863.
32 S. S. Nair, S. Sharma, Y. Pu, Q. Sun, S. Pan, J. Y. Zhu, Y. Deng and A. J. Ragauskas, *ChemSusChem*, 2014, **7**, 3513–3520.
33 T. Sathasivam, L. Hu, S. Sugiarto, Q. Dou, Z. Zhang, H. Ru Tan, Y. Leow, Q. Zhu, C. Ken Lee, H. Yu and D. Kai, *Chem.–Asian J.*, 2022, **17**, e202200671.
34 M. B. Agustin, M. Lehtonen, M. Kemell, P. Lahtinen, E. Oliaei and K. S. Mikkonen, *J. Environ. Manage.*, 2023, **330**, 117210.
35 S. Dadashi, S. M. Mousavi, Z. Emam-Djomeh and A. Oromiehie, *Int. J. Nanosci. Nanotechnol.*, 2014, **10**, 245–256.
36 D. A. D'Amico, M. L. Iglesias Montes, L. B. Manfredi and V. P. Cyras, *Polym. Test.*, 2016, **49**, 22–28.
37 I. Solala, M. C. Iglesias and M. S. Peresin, *Cellulose*, 2020, **27**, 1853–1877.
38 M. Österberg, J. Vartiainen, J. Lucenius, U. Hippi, J. Seppälä, R. Serimaa and J. Laine, *ACS Appl. Mater. Interfaces*, 2013, **5**, 4640–4647.
39 L. Bastarrachea, S. Dhawan and S. S. Sablani, *Food Eng. Rev.*, 2011, **3**, 79–93.
40 S. Shankar, J. P. Reddy and J.-W. Rhim, *Int. J. Biol. Macromol.*, 2015, **81**, 267–273.
41 L. Chen, C. Tang, N. Ning, C. Wang, Q. Fu and Q. Zhang, *Chin. J. Polym. Sci.*, 2009, **27**, 739–746.
42 K. R. Aadil, D. Prajapati and H. Jha, *Food Packag. Shelf Life*, 2016, **10**, 25–33.
43 R. Núñez-Flores, B. Giménez, F. Fernández-Martín, M. E. López-Caballero, M. P. Montero and M. C. Gómez-Guillén, *Food Hydrocolloids*, 2013, **30**, 163–172.
44 H. Zhao, Y. Zhu, H. Zhang, H. Ren and H. Zhai, *Int. J. Biol. Macromol.*, 2023, **242**, 124946.
45 Y. Inoue, K. H. Putera, L. van 't Hag and W. Batchelor, *Adv. Mater. Interfaces*, 2024, **11**, 2400455.
46 H. Lee, J. You, H.-J. Jin and H. W. Kwak, *Carbohydr. Polym.*, 2020, **232**, 115771.

47 E. Espinosa, I. Bascón-Villegas, A. Rosal, F. Pérez-Rodríguez, G. Chinga-Carrasco and A. Rodríguez, *Int. J. Biol. Macromol.*, 2019, **141**, 197–206.
48 A. A. Oun, G. H. Shin, J.-W. Rhim and J. T. Kim, *Food Packag. Shelf Life*, 2022, **34**, 100991.
49 A. El-Hadi, R. Schnabel, E. Straube, G. Müller and S. Henning, *Polym. Test.*, 2002, **21**, 665–674.
50 P. Anbukarasu, D. Sauvageau and A. Elias, *Sci. Rep.*, 2015, **5**, 17884.
51 H. Sadeghifar and A. Ragauskas, *Polymers*, 2020, **12**, 1134.
52 R. R. R. Ghadermazi, S. Hamdipour, K. Sadeghi, R. R. R. Ghadermazi and A. Khosrowshahi Asl, *Food Sci. Nutr.*, 2019, **7**, 3363–3377.
53 R. Vijayakumar, Y. Sivaraman, K. M. Pavagada Siddappa and J. P. R. Dandu, *Int. J. Polym. Anal. Charact.*, 2022, **27**, 99–110.
54 K. Crouvisier-Urion, P. R. Bodart, P. Winckler, J. Raya, R. D. Gougeon, P. Cayot, S. Domenek, F. Debeaufort and T. Karbowiak, *ACS Sustainable Chem. Eng.*, 2016, **4**, 6371–6381.
55 H. Sadeghifar, R. Venditti, J. Jur, R. E. Gorga and J. J. Pawlak, *ACS Sustainable Chem. Eng.*, 2017, **5**, 625–631.
56 H. Sadeghifar and D. S. Argyropoulos, *ACS Sustainable Chem. Eng.*, 2015, **3**, 349–356.
57 K. Li, W. Zhong, P. Li, J. Ren, K. Jiang and W. Wu, *Int. J. Biol. Macromol.*, 2023, **251**, 125992.
58 K. Crouvisier-Urion, A. Lagorce-Tachon, C. Lauquin, P. Winckler, W. Tongdeesoontorn, S. Domenek, F. Debeaufort and T. Karbowiak, *Food Chem.*, 2017, **236**, 120–126.
59 N. Balaban and A. Rasooly, *Int. J. Food Microbiol.*, 2000, **61**, 1–10.
60 S. Sanz, M. Giménez and C. Olarte, *J. Food Prot.*, 2003, **66**, 2203–2209.
61 K. F. El-Nemr, H. R. Mohamed, M. A. Ali, R. M. Fathy and A. S. Dhmees, *Int. J. Environ. Anal. Chem.*, 2020, **100**, 1578–1602.
62 W. Yang, H. Ding, G. Qi, C. Li, P. Xu, T. Zheng, X. Zhu, J. M. Kenny, D. Puglia and P. Ma, *React. Funct. Polym.*, 2021, **162**, 104873.
63 E. Gerbin, G. N. Rivière, L. Foulon, Y. M. Frapart, B. Cottyn, M. Pernes, C. Marcuello, B. Godon, A. Gainvors-Claisse, D. Crônier, A. Majira, M. Österberg, B. Kurek, S. Baumberger and V. Aguié-Béghin, *Int. J. Biol. Macromol.*, 2021, **181**, 136–149.
64 M. Chen, Y. Li, H. Liu, D. Zhang, Q.-S. Shi, X.-Q. Zhong, Y. Guo and X.-B. Xie, *Mater. Today Bio*, 2023, **18**, 100520.
65 K. Li, W. Zhong, P. Li, J. Ren, K. Jiang and W. Wu, *Int. J. Biol. Macromol.*, 2023, **252**, 126281.
66 B. Ndaba, A. Roopnarain, M. O. Daramola and R. Adeleke, *Sustainable Chem. Pharm.*, 2020, **18**, 100342.
67 A. G. Morena, A. Bassegoda, M. Natan, G. Jacobi, E. Banin and T. Tzanov, *ACS Appl. Mater. Interfaces*, 2022, **14**, 37270–37279.
68 H. Gao, M. Sun, Y. Duan, Y. Cai, H. Dai and T. Xu, *Int. J. Biol. Macromol.*, 2023, **246**, 125596.
69 M. Matos, F. C. Claro, T. A. M. Lima, F. Avelino, F. A. Hansel, G. M. Maciel, D. Lomonaco and W. L. E. Magalhães, *J. Anal. Appl. Pyrolysis*, 2021, **156**, 105175.
70 M. Mikulášová and B. Košíková, *Folia Microbiol.*, 1999, **44**, 669–672.
71 M. Peltzer, J. Wagner and A. Jiménez, *Food Addit. Contam.,: Part A*, 2009, **26**, 938–946.